Int. J. Electrochem. Sci., 13 **(2018)** 752 – 761, doi: 10.20964/2018.01.90

International Journal of
ELECTROCHEMICAL
SCIENCE
www.electrochemsci.org

Ag and $CoFe_2O_4$ co-sensitized TiO_2 nanowire for photocathodic protection of 304 SS under visible light

Zhehua Wen[1,2,4,a], *Ning Wang*[2,3,4,a], *Jing Wang*[2,4,*], *Baorong Hou*[1,2,4,*]

[1] Institute of Marine Science and Technology, Shandong University, Qingdao, 266237, China.
[2] Key Laboratory of Marine Environmental Corrosion and Bio-fouling, Institute of Oceanology, Chinese Academy of Sciences, Qingdao 266071, China.
[3] University of Chinese Academy of Sciences, Beijing 100049, China.
[4] Open Studio for Marine Corrosion and Protection, Qingdao National Laboratory for Marine Science and Technology, Qingdao, 266237, China.
[*]E-mail: baoronghou@163.com, jwang0501@126.com
[a] Equal contributions to this work.

Received: 15 September 2017 / *Accepted:* 13 November 2017 / *Published:* 16 December 2017

Ag and $CoFe_2O_4$ co-sensitized TiO_2 nanowire (NW) structures were fabricated by photoreduction deposition and hydrothermal methods. The morphology, chemical composition and optical absorption capabilities of the nanocomposites were systematically investigated by scanning electron microscopy (SEM), X-ray photoelectron spectroscopy (XPS) and UV–visible absorption spectra methods. The photo-induced open circuit potential (OCP) and photocurrent density were measured under visible light to evaluate the photocathodic protection effects of the nanocomposites for 304 SS in the presence and absence of illumination. The results indicated that the deposition of Ag and $CoFe_2O_4$ nanoparticles (NPs) shifted the light absorption of TiO_2 to the visible light region and enhanced the separation efficiency of the photogenerated charges. The nanocomposite exhibited more efficient photocathodic protection for 304 SS compared with pure TiO_2 under visible light.

Keywords: TiO_2; $CoFe_2O_4$; Ag; photocathodic protection

1. INTRODUCTION

Since Yuan and Tsujikawa reported that TiO_2 could offer photocathodic protection for Cu [1], the application of TiO_2 for the corrosion protection of metals has attracted great attention [2-8]. TiO_2 is a promising photoelectronic material because it shows a high photoelectric conversion efficiency, good chemical stability and is non-toxic. However, the wide bandgap of TiO_2 (3.2 eV) prevents the efficient absorption of sunlight in the visible light region and results in poor energy conversion efficiency. In

addition, the photoelectrochemical property of TiO_2 becomes invalid in the dark because of the recombination of the photogenerated charges. A considerable number of studies have been conducted to address these problems by compounding TiO_2 with other materials such as metals [9, 10], non-metals [11-13], and narrow bandgap semiconductor quantum dots [14]. Specifically, semiconductors can provide lower energy barriers, which offer opportunities for harvesting light energy in the visible light region of the solar spectrum. Some narrow bandgap semiconductors have been demonstrated as visible light sensitizers for TiO_2-based materials, such as ZnO, Cu_2O, PbS, CdS, CdTe and $CoFe_2O_4$ [15-20].

$CoFe_2O_4$, with a narrow bandgap of 1.13 eV, is an attractive material for modifying TiO_2 [20]. In recent years, many studies have shown that $CoFe_2O_4$ is a useful magnetic photocatalyst due to its utilization of visible light and good photochemical stability [21,22]. $CoFe_2O_4$-sensitized TiO_2 photoelectrodes have effectively extended the photoresponse of TiO_2 into the visible light region [23]. Ag is one of the most useful noble metals in decorating a TiO_2 nanostructure because Ag nanoparticles can extend the visible light response and enhance the absorption of TiO_2 [24-28]. In addition, between the Ag nanoparticles and TiO_2 nanostructure have a high Schottky barrier that can prohibit the recombination of photogenerated electrons and holes and thus promote the electron transfer process [29]. To the best of our knowledge, Ag and $CoFe_2O_4$ co-sensitized TiO_2 nanowire structures used for photocathodic protection have not been reported.

In this work, a TiO_2 nanowire structure on a Ti foil substrate was fabricated by a one-step electrochemical anodization method. Ag and $CoFe_2O_4$ co-sensitized TiO_2 nanowire structures were fabricated by photoreduction deposition and hydrothermal methods. The influences of the $AgNO_3$ concentration and $CoFe_2O_4$ reaction time on the photocathodic protection performance for 304 SS under visible light were studied.

2. EXPERIMENTAL

2.1. Preparation of the Ag/$CoFe_2O_4$/TiO_2 NWs and 304 SS electrodes

TiO_2 NWs were prepared by a one-step electrochemical anodization method. Prior to anodization, The Ti foils (30 mm × 10 mm of a 0.1 mm thickness; purity >99%) were ultrasonically cleaned in acetone, ethanol and deionized water for 10 min. The cleaned foil was conducted in a 2 M NaOH solution at 80°C for 180 min [30]. The anodizing cell used a conventional two-electrode system with a Pt foil as the counter electrode and a Ti foil as the working electrode. The constant voltage between two electrodes was 30 V. The as-anodized TiO_2 NWs were annealed at 450°C for 2 h in air at a heating rate of 5°C/min and naturally cooled down afterwards.

In a typical experimental procedure for the preparation of the $CoFe_2O_4$-sensitized TiO_2 electrode, 5.0 mmol of $FeCl_3.H_2O$ and 2.5 mmol of $CoCl_2.6H_2O$ were dissolved into 40.0 mL of H_2O, adding 1.0 mL of acetylacetone drop by drop as the stabilized reagent. Then, 45.0 mmol of urea was added slowly under stirring, and the mixture was stirred for approximately 30 min [23]. The mixed solution was transferred in a Teflon-lined stainless-steel autoclave. Subsequently, the annealed TiO_2

electrode was placed at an angle against the wall of the Teflon-liner. Then, the autoclave was sealed and maintained at 180°C for 3, 6, 9 and 12 h in an oven. After being cooled to room temperature naturally, the electrode was rinsed with deionized water and absolute ethanol and dried at 60°C for 6 h.

Ag NWs were synthesized by a photoreduction method. Typically, the as-obtained $CoFe_2O_4/TiO_2$ NWs were first immersed in various concentrations of $AgNO_3$ solution for 30 min and then illuminated under UV light (UVC220-2H15W) for 30 min. Finally, the specimens with various $Ag/CoFe_2O_4/TiO_2$ films were rinsed and dried in air [31].

The nominal composition of 304 SS (in wt.%) is 0.08 C, 1.86 Mn, 0.72 Si, 0.035 P, 0.029 S, 18.25 Cr, 8.5 Ni, and the remainder as Fe. The 304 SS electrode was made by embedding a square of 304 SS in epoxy resin, and the exposed area for testing was 10 mm × 10 mm. This electrode was polished with SiC paper up to a 2400 grit size. The as-received electrode was ultrasonically cleaned in analytical grade ethanol for 5 min.

2.2. Characterization

The as-obtained samples were characterized by X-ray photoelectron spectroscopy (XPS, the American Thermo-VG Scientific ESCALAB 250 XPS system, Al Kα radiation and C 1s peak (284.6 eV) as a reference). The morphologies and microstructures of the samples were observed using a scanning electron microscope (SEM, Hitachi S-4800, Japan) that operated at 25 kV. The UV–visible (UV–vis) absorption spectra were recorded with a UV–vis spectrophotometer (Cary 5000, Varian, USA).

2.3. Photocathodic protection properties

The photocathodic protection properties of the 304 SS steel were evaluated under visible light (λ > 400 nm). The experiments were performed at room temperature on the PARSTAT P4000+ (Advanced Measurement Technology, USA). The Ag/ $CoFe_2O_4$/ TiO_2 photoelectrode was placed in the photoanode cell, whereas the 304 SS was placed in the corrosion cell. The Nafion film allows conduction between electrolyte solutions in these two cells. The visible light source was a 300 W Xe arc lamp (power energy density = 100 mW/cm^2) (CEL-HXF300, Zhongjiao, China). The $Ag/CoFe_2O_4/TiO_2$ photoelectrode and 304 SS were coupled and connected to the working electrode interface of the potentiostat to measure their open-circuit potentials (OCPs). The saturated calomel electrode (SCE) served as reference electrodes. The electrolyte was a 3.5 wt% NaCl solution in the corrosion cell and a 0.25 M Na_2SO_4 solution in the photoanode cell.

The photocurrent densities of the samples were measured with the P4000+ (Advanced Measurement Technology, USA) using a conventional three-electrode system. The Ti foil coated with a thin layer of $Ag/CoFe_2O_4/TiO_2$ composites was used as the working electrode. The SCE and Pt foils served as reference and counter electrodes, respectively. The visible light excitation source was a 300-W Xe arc lamp (power energy density = 100 mW/cm^2) equipped with a UV cutoff filter (λ > 400 nm). The measurements were performed at ambient temperature in a 0.25-M Na_2SO_4 aqueous electrolyte.

3. RESULTS AND DISCUSSION

3.1. Photocathodic protection performance (OCP measurements)

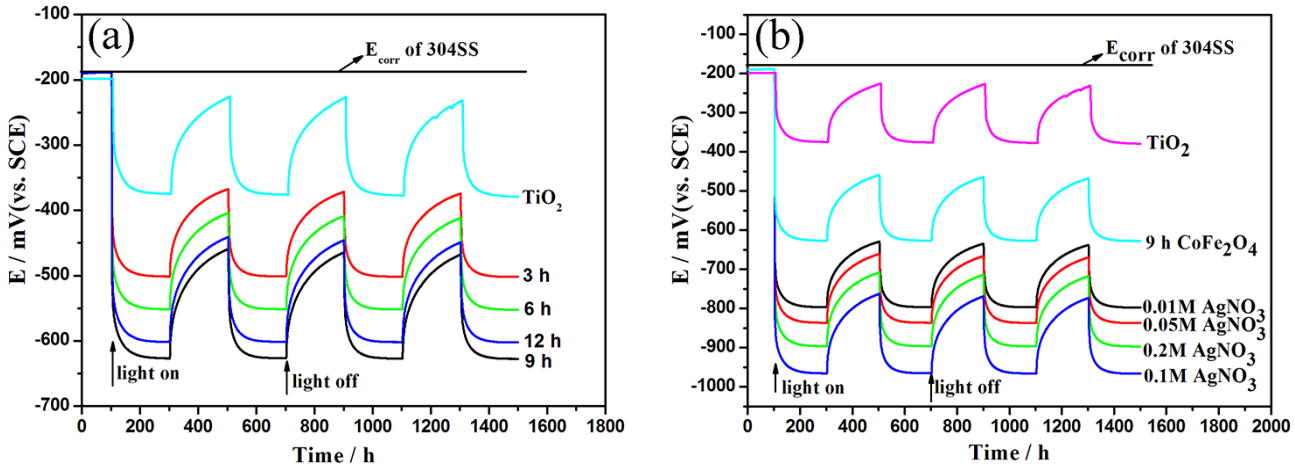

Figure 1. OCP variations in the 304 SS electrode coupled with $CoFe_2O_4/TiO_2$ NWs (a) and $Ag/CoFe_2O_4/TiO_2$ NWs (b) with and without illumination ($\lambda > 400$ nm).

Fig. 1 shows the OCP variations in the 304 SS electrode coupled with $CoFe_2O_4/TiO_2$ and $Ag/CoFe_2O_4/TiO_2$ photoelectrodes with and without illumination. When the light was turned on, the OCP of all the photoelectrodes exhibited a markedly negative shift. The stable value of the OCP under illumination was recorded as the photopotential. The photopotential values of the coupled $CoFe_2O_4/TiO_2$ electrodes were more negative than that of pure TiO_2. This result indicated that $CoFe_2O_4/TiO_2$ exhibited enhanced photocathodic protection capabilities compared with that of pure TiO_2 under visible light. Furthermore, when Ag NPs are deposited on the surface of the $CoFe_2O_4/TiO_2$ electrodes, the photopotential exhibited more negative values than those of the pure TiO_2 and $CoFe_2O_4/TiO_2$ photoelectrodes. As the reaction time increased, the photopotentials of the coupled electrodes shifted negatively until the reaction time reached 9 h, where the photogenerated cathodic protection property was the best. The photopotential values of the coupled electrodes that correspond to the $CoFe_2O_4/TiO_2$ electrodes prepared for 9 h were stabilized at approximately −625 mV, whereas those of the $CoFe_2O_4/TiO_2$ samples prepared for 3, 6 and 12 h were stabilized at approximately −500, −550 and −590 mV, respectively. The adsorption of photons grew in number as the reaction time increased. However, the adsorption was saturated when the deposition film was thicker than the light penetration depth [32]. The results were very consistent with those of the photoelectrochemical experiments. After the light was off, the OCP of the coupled $CoFe_2O_4/TiO_2$ electrodes increased quickly and remained in a narrow range of −360 mV to −470 mV, which was still far below that of the corrosion potential of 304 SS. This result demonstrated that the $CoFe_2O_4$ NPs significantly improved the photocathodic protection performance of the TiO_2 photoanode. With increasing $AgNO_3$ concentration, the photopotentials of coupled electrodes shifted negatively until the $AgNO_3$ concentration reached 0.1 M, where the photogenerated cathodic protection property was the best. With increasing Ag content, there are excess Ag NP recombination sites of the photoinduced charges

[31]. Thus, Ag/$CoFe_2O_4$/TiO_2 was prepared for a $CoFe_2O_4$ reaction time of 9 h, and a $AgNO_3$ concentration of 0.1 M exhibited high photocathodic protection. This experiment selected a $CoFe_2O_4$ reaction time of 9 h, and a $AgNO_3$ concentration of 0.1 M to prepare the $CoFe_2O_4$/TiO_2 electrodes for SEM, XPS and UV−vis analyses.

3.2. SEM and XPS analyses

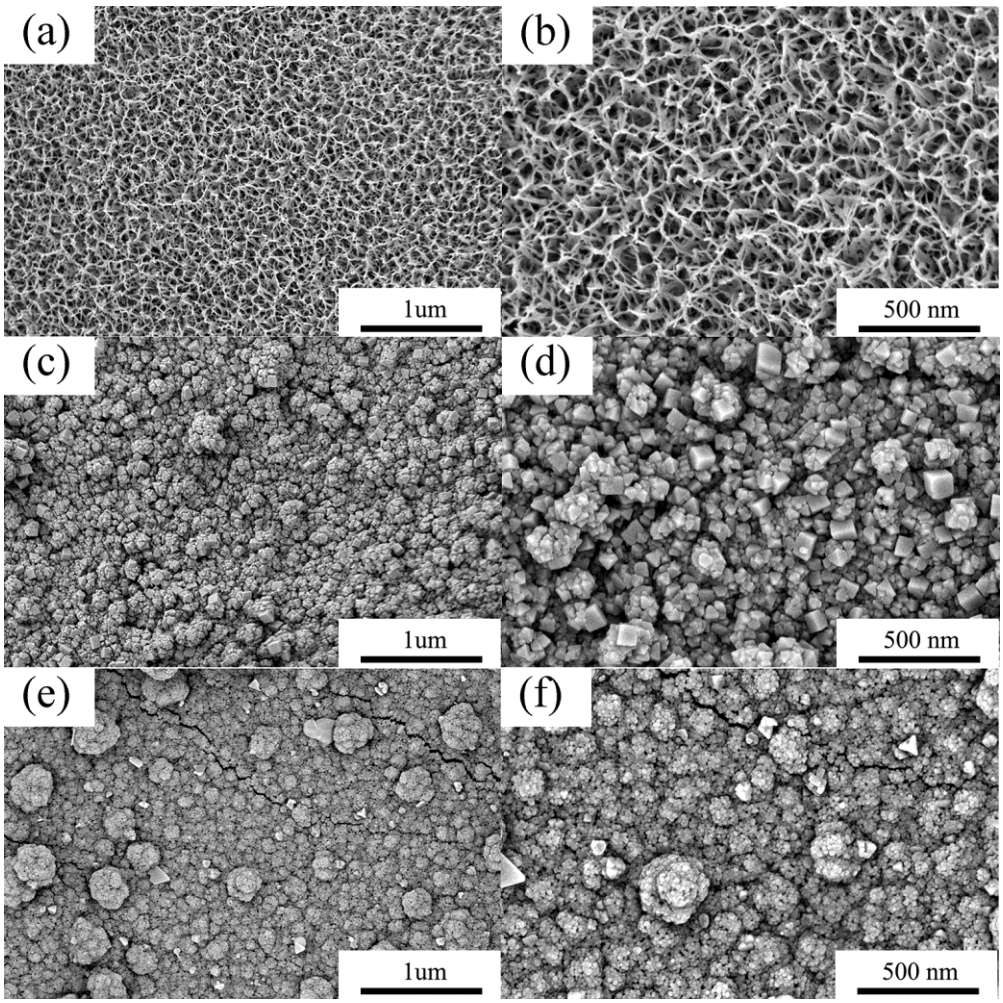

Figure 2. SEM images of pure TiO_2 (a, b), $CoFe_2O_4$/TiO_2 NWs with the $CoFe_2O_4$ reaction time of 9 h (c, d) and Ag/$CoFe_2O_4$/TiO_2 NWs with $CoFe_2O_4$ reaction time of 9 h, $AgNO_3$ concentration of 0.1 M (e, f).

The surface morphologies of the prepared photoanodes are shown in Fig. 2. Pure TiO_2 prepared by a one-step electrochemical anodization method was composed of a high-density and a uniform nanowire structure (Fig. 2a). The enlarged version of the framed area reveals that these nanowires connect with each other to form a net-like structure (Fig. 2b). After the deposition of $CoFe_2O_4$ on the TiO_2, the $CoFe_2O_4$ NPs well covered the surface and inner part of the TiO_2 nanowire, which suggests that the large surface area of the TiO_2 NW could facilitate complete contact of TiO_2 with the

nanoparticles. In Fig. 2e and Fig. 2f, it is obvious that after Ag NP deposition, compared with Fig. 2c and Fig. 2d, that the Ag NPs are deposited on the surface of $CoFe_2O_4/TiO_2$ NWs structure.

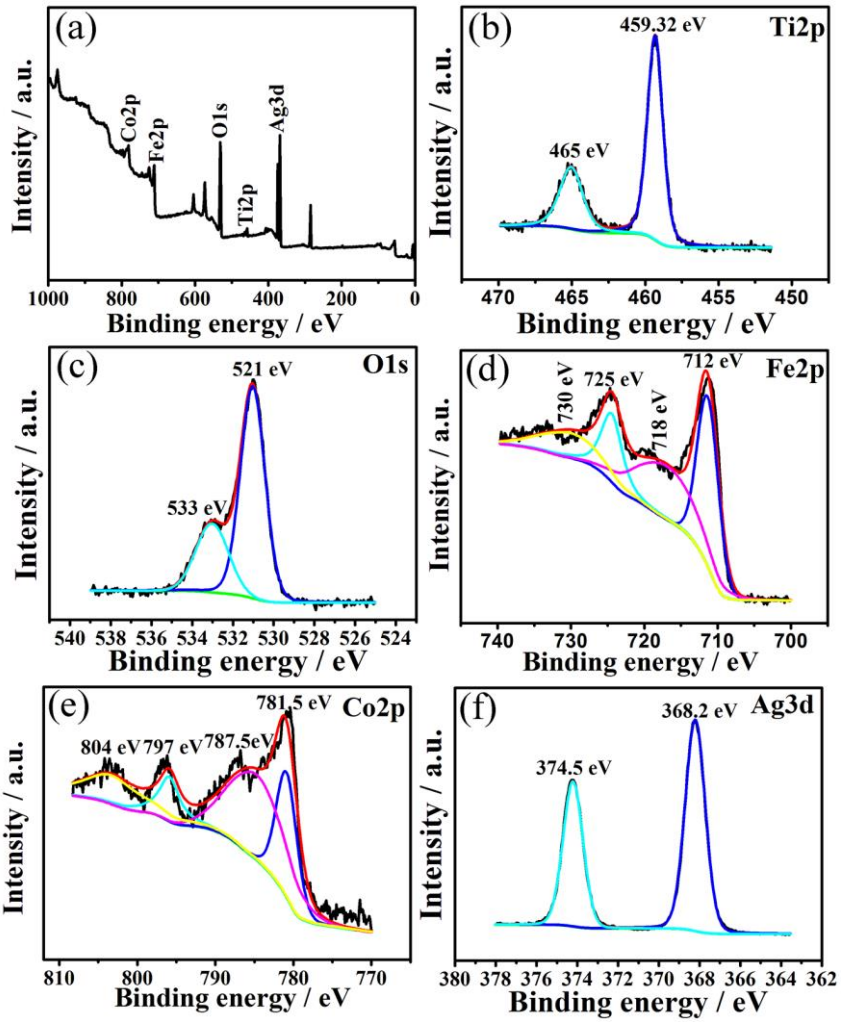

Figure 3. XPS survey spectra of $Ag/CoFe_2O_4/TiO_2$ (a), and high-resolution XPS spectra of Ti 2p (b), O 1s (c), Fe 2p (d), Co 2p (e) and Ag 3d (f).

Fig. 3 demonstrates the XPS spectra of the $Ag/CoFe_2O_4/TiO_2$ nanocomposite. Fig. 3a shows the survey scan spectrum of $Ag/CoFe_2O_4/TiO_2$. The results indicate the clear presence of Ti, O, Fe, Co and Ag. As shown in Fig. 3b, the Ti 2p spectrum has two peaks centred at 459.32 and 465 eV, corresponding to Ti 2p3/2 and Ti 2p1/2, respectively [31]. These peaks indicate that the main chemical state of Ti in this composite has a +4 valence. As shown in Fig. 3d, the peaks centred at 712 and 725 eV correspond to Fe 2p3/2 and Fe 2p1/2, respectively. In addition, the peaks centred at 718 and 730 eV come from the Fe3+ satellite. These peaks indicate that the main chemical state of Fe in this composite has a +3 valence [20]. In Fig. 2e, the Co 2p spectrum has four peaks centred at 787.5 and 804 eV, corresponding to Co 2p3/2 and Co 2p1/2, respectively. These peaks indicate that the main chemical state of Co in this composite exhibits a +2 valence [20]. Fig. 2f shows the high-resolution Ag 3d spectrum. The two peaks centred at 368.2 and 374.5 eV belong to Ag 3d5/2 and Ag 3d1/2, respectively

[32]. Similar results have obtained in others' studies [33-37]. For example, Gupta and co-workers [33] have synthesized a novel $CoFe_2O_4$@TiO_2/rGO nanocomposite, the peaks centred at 718.3 and 722.1 eV correspond to Fe 2p3/2 and Fe 2p1/2, respectively. In addition, the Co 2p spectrum has two peaks centred at 779.9 and 802.4 eV, corresponding to Co 2p3/2 and Co 2p1/2. In Ma's study [36], the two peaks centred at 366.8 and 372.8 eV belong to Ag 3d5/2 and Ag 3d1/2, respectively. These results demonstrated that Ag and $CoFe_2O_4$ NPs have been successfully synthesized.

3.2. UV−vis optical absorption and photocurrent density analysis

The UV–vis absorption spectra of pure TiO_2, $CoFe_2O_4/TiO_2$, and $Ag/CoFe_2O_4/TiO_2$ are shown in Fig. 4. Pure TiO_2 exhibited its absorption edge at approximately 380 nm because of its intrinsic bandgap absorption. Comparatively, after being coupled with the Ag and $CoFe_2O_4$ NPs, the light absorption edge of the $Ag/CoFe_2O_4/TiO_2$ composite exhibited a significant redshift to the visible light region and the ultraviolet light absorption was also enhanced. Some related and relevant papers have obtained the same results [38-42]. For example, Li and co-workers [39] reported that the intensity of absorbance of the $CoFe_2O_4/TiO_2$ heterogeneous significantly increases and the absorption edge has broadened to the visible light region. In Peng's study [42], after loading Ag NPs, Ag/TiO_2 NWs exhibit an obvious absorption spectrum with a peak of about 580 nm. These results indicated that the Ag and $CoFe_2O_4$ NPs enhanced light absorption in both the UV and visible light regions and shifted the absorption range into the visible light region.

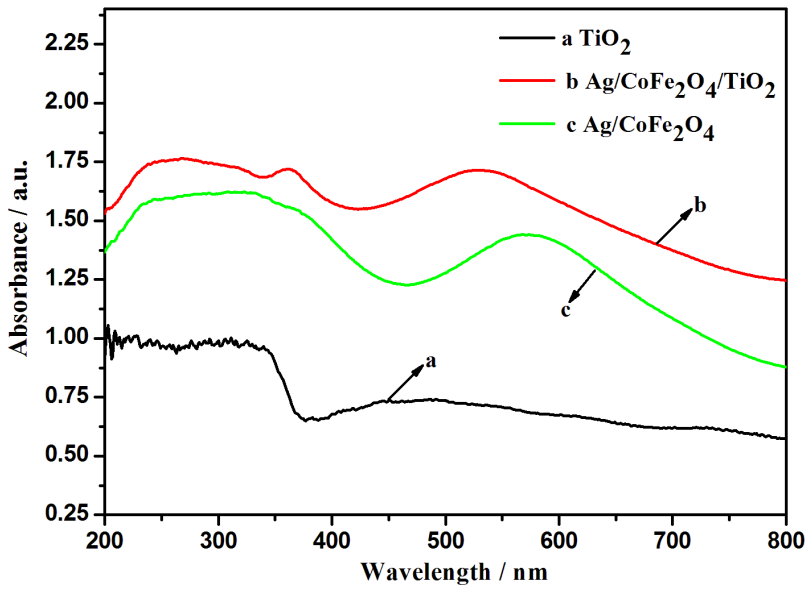

Figure 4. UV–vis absorption spectra of pure TiO_2, $CoFe_2O_4/TiO_2$ NWs and $Ag/CoFe_2O_4/TiO_2$ NWs.

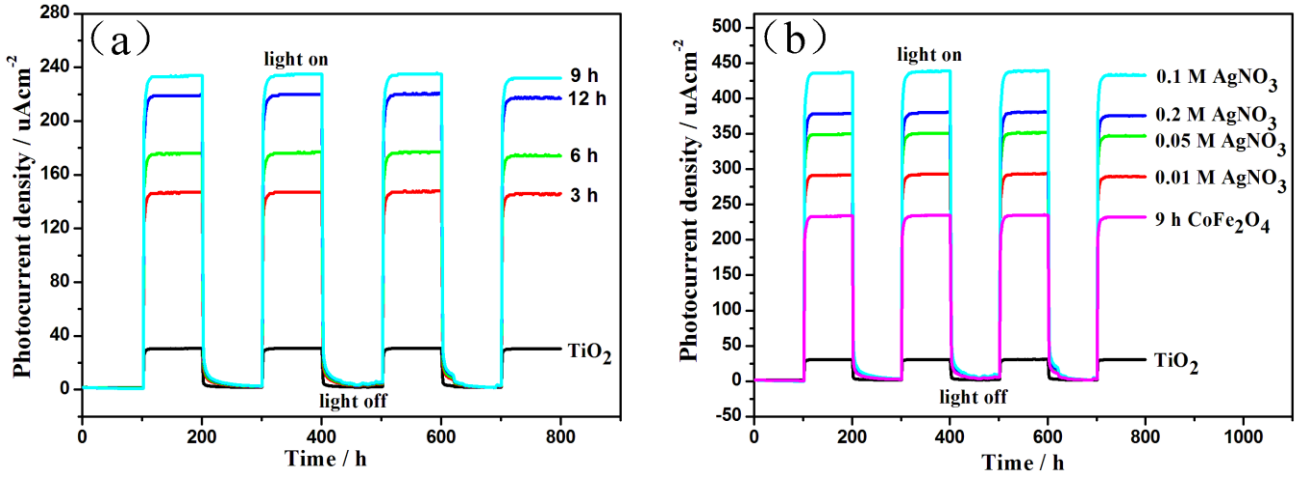

Figure 5. Current–time (*I-t*) curves of $CoFe_2O_4/TiO_2$ (a) and $Ag/CoFe_2O_4/TiO_2$ NWs (b) with and without illumination (λ > 400 nm).

Fig. 5. demonstrates the transient photocurrent density at various $CoFe_2O_4$ reaction times and $AgNO_3$ concentrations. From Fig. 5, we determined that the photocurrent of TiO_2 nanotubes under visible light irradiation was greatly enhanced after the deposition of the Ag and $CoFe_2O_4$ NPs. In Fig. 5a, with an increase in $CoFe_2O_4$ reaction time, the photocurrent density of the composite was revealed that the photocurrent density first increased and then decreased. A reaction time of 9 h showed the highest photocurrent density of 238 μA cm^{-2}, which is approximately 7.4 times greater than that of pure TiO_2 (32 μA cm^{-2}). Furthermore, when the Ag NPs were deposited on the surface of the $CoFe_2O_4/TiO_2$ electrodes, the photocurrent density of the $Ag/CoFe_2O_4/TiO_2$ electrodes also first increased and then decreased. A $AgNO_3$ concentration of 0.1 M showed the highest photocurrent density of 440 μA cm^{-2}, which is approximately 14 times greater than that of the pure TiO_2 (32 μA cm^{-2}). These results further revealed that the Ag and $CoFe_2O_4$ semiconductors are efficient photosensitizers in the composites, and the combination of TiO_2 with the nanoparticles can improve the photocurrent efficiency of the composite.

According to OCP analysis, an increase in the $CoFe_2O_4$ reaction time was useful for the effective separation of photogenerated electron-hole pairs and faster charge transfer at the $CoFe_2O_4/TiO_2$ interface. The low photocurrent density of $CoFe_2O_4/TiO_2$ prepared for 3 h (147 μA cm^{-2}) may be due to the $CoFe_2O_4$ nanoparticle charge transfer limit and parts of the semiconductor surface could not be excited under visible light irradiation. However, for the $CoFe_2O_4/TiO_2$ samples prepared for 12 h, the photocurrent was approximately 220 μA cm^{-2}. These results could be because excessive $CoFe_2O_4$ nanoparticles deposited on the TiO_2 surface could increase the recombination of charge carriers, thereby preventing the charge carrier transfer across the thick $CoFe_2O_4$ film. With an increasing $AgNO_3$ concentration, the photocurrent densities of the $Ag/CoFe_2O_4/TiO_2$ electrodes first increased and then decreased. With increasing Ag content, the photocurrent is inclined to saturate when the Ag content increases to a certain value, which produces excess Ag NP recombination sites for the photoinduced charges [32]. Thus, $Ag/CoFe_2O_4/TiO_2$ prepared for a $CoFe_2O_4$ reaction time of 9 h, and a 0.1 M $AgNO_3$ concentration has a high photoelectrochemical efficiency.

4. CONCLUSIONS

In summary, Ag and $CoFe_2O_4$ co-sensitized TiO_2 NW structures were successfully fabricated by photoreduction deposition and hydrothermal methods. Ag and $CoFe_2O_4$ NPs enhanced the light absorption of in both the UV and visible light regions and shifted the absorption range to the visible light region. $Ag/CoFe_2O_4/TiO_2$ exhibited a higher photocurrent density and photogenerated cathodic protection compared with those of pure TiO_2. $Ag/CoFe_2O_4/TiO_2$ was prepared for a $CoFe_2O_4$ reaction time of 9 h, and a 0.1 M $AgNO_3$ concentration exhibited the optimal photocathodic protection for 304 SS under visible light.

ACKNOWLEDGEMENTS
This work was financially supported by the Strategic Pilot Science and Technology of Chinese Academy of Sciences (Class A) (XDA13040401).

References

1. J.N. Yuan, S. Tsujikawa, *J. Electrochem. Soc*., 142 (1995) 3444-3450.
2. R. Subasri, S. Deshpande, S. Seal, T. Shinohara, *Electrochem. Solid-State Lett*., 9 (2006) B1-B4.
3. R. Subasri, T. Shinohara, K. Mori, *J. Electrochem. Soc*., 152 (2005) B105-B110.
4. C.Y. Mo, Y.S. Zheng, F.L. Wang, Q. Mo, *Int. J. Electrochem. Sci*., 10(2015)7380-7391.
5. L. Curkovic, H.O. Curkovic, S. Salopek, M.M. Renjo, S. Segota, *Corros. Sci*., 77 (2013) 176-184.
6. X.Q. Guo, W. Liu, L.X. Cao, G. Su, H.M. Xu, B.H. Liu, *Appl. Surf. Sci*., 283 (2013) 498-504.
7. C.X. Lei, H. Zhou, C. Wang, Z.D. Feng, *Electrochim. Acta*, 87 (2013) 245-249.
8. L. Zhang, X.T. Wang, F.G. Liu, H.F. Sun, H. Li, Q.Y. Wei, B.R. Hou, *Mater. Lett*., 143(2015)116-119.
9. X.F. Lei, X.X. Xue, H. Yang, *Appl. Surf. Sci*., 321 (2014) 396-403.
10. D.W. Ding, K. Liu, S.N. He, C.B. Gao, Y.D. Yin, *Nano Lett*., 14 (2014) 6731-6736.
11. P.H. Wang, P.S. Yapa, T.T. Lim, *Appl. Catal.,* A, 399 (2011) 252-261.
12. H.U. Lee, S.C. Lee, S. Choi, B. Son, S.M. Lee, H.J. Kim, J. Lee, *Chem. Eng. J*., 228 (2013) 756-764.
13. H. Khalilian, M. Behpour, V. Atouf, S.N. Hosseini, *Sol. Energy*, 112 (2015) 239-245.
14. N. Yao, C.C. Wu, L.C. Jia, S. Han, B. Chi, J. Pu, L. Jian, *Ceram. Int*., 38 (2012) 1671-1675.
15. C.B. Murray, D.J. Norris, M.G. Bawendi, *J. Am. Chem. Soc*., 115 (1993) 8706.
16. C.C. Pei, W.W. Leung, *Sep. Purif. Technol*., 114 (2013) 108-116.
17. S.S. Zhang, S.Q. Zhang, F. Peng, H.M. Zhang, H.W. Liu, H.J. Zhao, *Electrochem. Commun*., 13 (2011) 861-864.
18. R. Brahimi, Y. Bessekhouad, A. Bouguelia, M. Trari, *J. Photoch. Photobio*., 194 (2008) 173-180.
19. C.B. Wang, Z.F. Jiang, L. Wei, Y.X. Chen, J. Jiao, M. Eastman, H. Liu, *Nano Energy*, 1 (2012) 440-447.
20. L.Q. Jing, Y.G. Xu, S.Q. Huang, M. Xie, M.Q. He, H. Xu, H.M. Li, Q. Zhang, *Appl. Catal*., B, 119 (2016) 11-12.
21 H. Gong, W. Chu, *J. Hazard. Mater*., 314(2016)197-203.
22 C.J. Li, J.N. Wang, B. Wang, J.R. Gong, Z. Lin, *Mater. Res. Bull*., 47 (2012) 333-337.
23 B.X. Lei, W. Sun, Z.F. Sun, *Mater. Res. Bull*., 48 (2013) 3625-3629.
24 Y.K. Lai, H.F. Zhuang, K.P. Xie, D.G. Gong, Y.X. Tang, L. Sun, C.J. Lin, Z. Chen, *New J. Chem*., 34 (2010) 1335-1340.

25 C.X. Feng, J.W. Zhuang, R. Lang, Z.S. Jin, Z.S. Wu, Z.J. Zhang, *Appl. Surf. Sci*., 257 (2011) 1864-1870.
26 F. Wu, X.Y. Hu, J. Fan, E.Z. Liu, T. Sun, L.M. Kang, W.Q. Hou, C.J. Zhu, H.C. Liu, *Plasmonics*, 8 (2013) 501-508.
27 D.Y. Pan, J.H. Li, L. Wang, C. Xi, Q. Xue, M.H. Wu, Z. Li, *Mater. Lett*., 100 (2013) 82-85.
28 K.S. Chen, X.R. Feng, R. Hu, Y.B. Li, K. Xie, Y. Li, H.S. Gu, *J. Alloys Compd*., 554 (2013) 72-79.
29 C.X. Xu, P.W. Chen, J.J. Liu, H. Yin, X. Gao, X.F. Mei, *J. Alloys Compd*., 679 (2016) 463-469.
30 X.W. Huang, Z. J. Liu, *J. Mater. Sci. Technol*., 30 (2014) 878-883.
31 J.H. Kong, C.X. Song, W. Zhang, Y.H. Xiong, M. Wan, Y.Q. Wang, *Superlattices Microstruct*., 109(2017)579-587.
32 H. Li, X.T. Wang, Y. Liu, B.R. Bao, *Corros. Sci*., 82 (2014) 145-153.
33 V.K. Gupta, T. Eren, N. Atar, M.L. Yola, C. Parlak, H. Karimi-Maleh, *J. Mol. Liq*., 208(2015)122-129.
34 X. Zhang, Y. Huang, X.F. Chen, C. Li, J.J. Chen, *Mater. Lett*., 158(2015)380-383.
35 H.J. Liang, Z.C. Jia, H.C. Zhang, X.B. Wang, J.J. Wang, *Appl. Surf. Sci*., 422(2017)1-10.
36 J.T. Park, C.S. Lee, C.H. Park, J.H. Kim, *Chem. Phys. Lett*., 685(2017)119-126.
37 C. Ma, X.F. Wang, H. Luo, D. Zhang, *J. Mater. Sci.: Mater. Electron*., 28(2017)10715-10719.
38 B.N. Shi, J.F. Wan, C.T. Liu, X.J. Yu, F.W. Ma, *Mat. Sci. Semicon. Proc*., 37(2015)241-249.
39 C.J. Li, J.N. Wang, B. Wang, J.R. Gong, Z. Lin, *J. Nanosci. Nanotechno*., 12(2012)2496-2502.
40 Y. Liu, H.Z. He, J. Li, W.Z. Li, Y.H. Yang, Y.M. Li, Q.Y. Chen, *RSC Adv*., 5(2015)99378-99384.
41 L. Lu, Y.N. Gao, F.Z. Wang, P. Liu, S.G. Hu, *Chinese J. Catal*., 38(2017)357-364.
42 C.C. Peng, W.Z. Wang, W.W. Zhang, Y.J. Liang, L. Zhuo, *Appl. Surf. Sci*., 420(2017)286-295.

© 2018 The Authors. Published by ESG (www.electrochemsci.org). This article is an open access article distributed under the terms and conditions of the Creative Commons Attribution license (http://creativecommons.org/licenses/by/4.0/).